Morphology control

DOI: 10.1002/smll.200600219

Shape-Controlled Growth of Micrometer-Sized Gold Crystals by a Slow Reduction Method**

*Xiaogang Liu, Nianqiang Wu, Benjamin H. Wunsch, Robert J. Barsotti Jr., and Francesco Stellacci**

Molecular recognition events that occur at the interface between organic molecules and inorganic surfaces play an important role in a broad range of technologically and scientifically relevant processes including crystal growth, heterogeneous catalysis, and the development of sensor systems based on bioinspired functional materials.[1–5] For example, selective recognition of specific crystalline surfaces has recently led to the synthesis of a wide range of anisotropic nanocrystals such as rods,[6–10] cubes,[11–13] wires,[14,15] prisms,[16–19] and branched multipods.[20–24] Crystal growth rates, and ultimately equilibrium shapes, are strongly influenced by the preferential binding of crystallographic planes, a phenomenon that is thought to affect the surface free energies and to alter the relative stabilities of different planes.[25,26] The mechanism of formation of these interesting nanoparticles has been thoroughly investigated in recently years.[27] To date, little is known on the evolution in size and shape of individual crystals from the nanometer to the micrometer scale, a size where characterization methods for larger crystals are more established.[28,29] Undoubtedly there is a lack of synthetic methods for producing micrometer-scale crystals with shape control, even though large crystals could be useful tools for understanding crystal-growth mechanisms, and may find uses in microelectronic systems.[30,31]

Here we present a general and versatile method for the synthesis of micrometer-sized gold crystals with shapes ranging from three-dimensional (3D) triangles, octahedra, and pentagonal decahedra to two-dimensional (2D) plates and one-dimensional (1D) nanowires. These well-defined morphologies were obtained by controlling the relative growth rates of the crystal planes by the selective use of capping ligand mixtures. The size transition and shape evolution of the crystals were monitored by electron microscopy, X-ray powder diffraction (XRD), and X-ray photoelectron spectroscopy (XPS).

The method involves the slow reduction of gold precursors by amine molecules. It is known that certain amines function as weak (and thus slow) reductants and as metal coordination ligands for metal complexes in solution.[32] Both of these properties should contribute to a slow rate of particle growth and hence to the formation of large particles. We have used various amine combinations as starting materials in combination with a "Au(III) source" for the synthesis of gold particles. By changing the composition of the amine ligand mixture, micrometer-sized crystals with different feature shapes and sizes can be obtained.

It was reported that spherical gold nanoparticles can be obtained by refluxing ($\approx$110 °C) a toluene solution of $H[AuCl_4]$ with either oleylamine or dodecylamine (DA).[32] Using the latter, we have found that nanoparticles of $\approx$18 nm in diameter form in 34 h. In contrast, we have found that when a toluene solution of $H[AuCl_4]$ (18 mg; 0.045 mmol) and DA (42 mg; 0.226 mmol) is heated only at 81 °C for 34 h a yellow shining precipitate is formed. Scanning electron microscopy (SEM) images show that the precipitate consists of polyhedral particles (e.g., octaheadra, rhombododecahedra, truncated pentagonal decahedra, etc.) with submicrometer ($\approx$650 nm) dimensions (Figure 1 A). It is evident that the lower temperature of reaction favors the growth of large particles. The formation of variously shaped particles composed of a relatively equal distribution of three crystallographic planes ({111}, {100}, and {110}) of face-centered cubic (fcc) gold is attributed, in large part, to a nonspecific interaction of the primary amine (DA) with these three planes.

The shape of the particles is determined by the relative growth rates on particular crystallographic planes during the growth process. To control the relative growth rates of different crystallographic facets and consequently tune the morphology of the gold crystals, a quaternary amine salt (didodecyldimethylammonium bromide: DDAB) was used in combination with a primary amine (DA). Figure 1 B–D shows the morphological change of gold crystallites prepared at 81 °C as a function of the quaternary amine to primary amine molar ratio (γ). In Figure 1 B, the particle morphology exhibits predominantly triangular, octahedral, and pentagonal decahedral outlines with smooth vertexes and edges as γ equals 1.25. These surface morphologies are comprised of {111}-dominant facets, indicating specific recognition of the {111} plane by the quaternary amine that lowers the surface energy and stabilizes this plane.[18] Upon further increasing the concentration of the quaternary amine, large crystals in the forms of faceted triangular or hexagonal platelets emerged (γ=2) and became the predominant product at γ=3 (Figure 1 C and D, respectively). The platelets have an averaged lateral dimension of 7 μm and an averaged thickness of 140 nm. Thus, {111} facets constitute $\approx$96 % of the total surface area, on average.

Varying the primary amine from DA to many other primary amines (including oleyamine, octadecylamine, and 4-

[*] Dr. X. Liu, B. H. Wunsch, R. J. Barsotti Jr., Prof. F. Stellacci
Department of Materials Science and Engineering
Massachusetts Institute of Technology
77 Massachusetts Avenue, Room 13-4053
Cambridge, MA 02139 (USA)
Fax: (+1) 617-324-2500
E-mail: frstella@mit.edu
Prof. N. Wu
Department of Mechanical & Aerospace Engineering
West Virginia University, P.O. Box 6106
Morgantown, WV 26506 (USA)

[**] F.S. is grateful to 3M and DuPont for the Young Faculty Awards. We thank Prof. L. D. Marks, J. Adario, and D. Bell for helpful discussions and technical assistance.

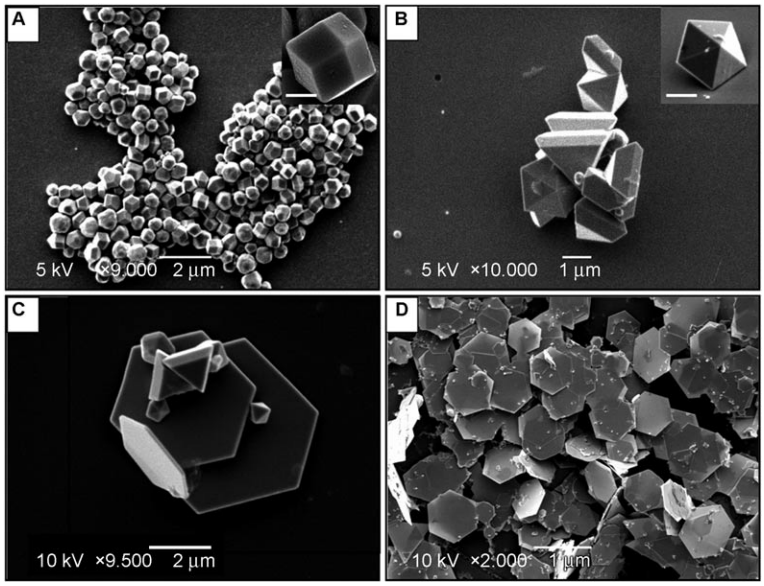

Figure 1. SEM images of gold crystals synthesized via combinations of amine molecules. A) DA-coated particles (Inset: HREM image of a rhombododecahedral particle. Scale bar: 200 nm). B) DDAB/DA-coated particles at $\gamma = 1.25$ (Inset: HREM image of a pentagonal decahedron. Scale bar: 1 μm). C) DDAB/DA-coated particles ($\gamma = 2$). D) DDAB/DA-coated platelets ($\gamma = 3$).

phenylbutylamine) resulted in a similar shape-evolution pattern to that of DA. Combinations of various types of amines (primary, secondary, tertiary, and quaternary amines) could yield gold crystals with controlled morphologies and sizes. It should be noted that ammonium counterions (e.g., bromide or chloride) may play an important role in promoting the formation of anisotropic particles. For instance, octahedral gold particles at the micrometer-length scale were prepared in nearly quantitative yield by using a binary mixture of DA and tridodecylmethylammonium chloride (TDAC) in a 1:1 molar ratio (Figure 2A). Under similar conditions the use of bromide counterions leads to a mixture of particles of various shapes. It is also possible to synthesize gold plates with control over feature sizes from a few micrometers up to 100 μm by varying the composition of the amine ligand mixture (Figure 2B–D).

To demonstrate the flexibility of this approach, we attempted to prepare 1D nanostructures. The synthesis of 1D nanostructures such as rods and wires has received enormous attention owing to their interesting physical properties and importance in the fabrication of nanoscale devices.[14] Although several procedures exist for preparing Au 1D nanostructures including electrochemical deposition in templates,[15] photochemical synthesis,[7] and seed-mediated growth,[6] there are very few solution-phase-based methods that allow for scalable synthesis of Au nanowires with high aspect ratios. We found that a combination of a tertiary amine (trioctylamine) and DDAB (1:1 molar ratio) as the ligand precursors in the presence of $H[AuCl_4]$ under slow growth conditions resulted in the formation of uniform nanowires of ≈ 150 nm diameter and ≈ 80 μm length with an averaged aspect ratio of ≈ 500 (Figure 3A and B). Upon evaporation of solvent, the nanowires tend to assemble into "stacks" on the substrate (Figure 3B). The nanowires consist of an elongated cyclic pentatetrahedral twin crystal in which five {111} twin boundaries are arranged to the [110] preferred orientation along the fivefold axis (Figure 3B, inset). Formation of the anisotropic nanowires can be attributed to the coupling of an intrinsic structural mechanism (multiple twinning) and extrinsic surface modification (se-

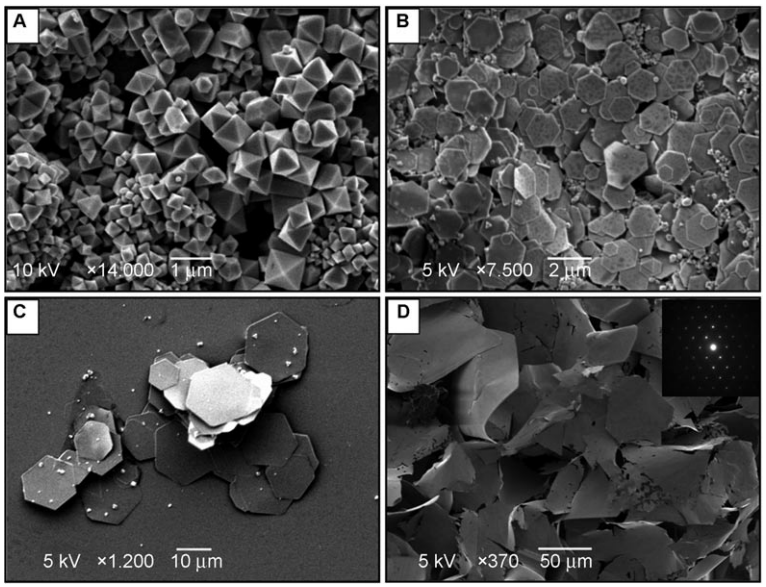

Figure 2. SEM images of gold crystals synthesized via combinations of amine molecules: A) TDAC/DA-coated octahedra (1:1 molar ratio). B) TDAC/DA-coated gold plates (1.2:1 molar ratio). C) DDAB/DA-coated plates (4:1 molar ratio). D) DDAB/dibutylamine-coated thin plates (1:1 molar ratio). Inset: representative electron diffraction pattern of the thin plates.

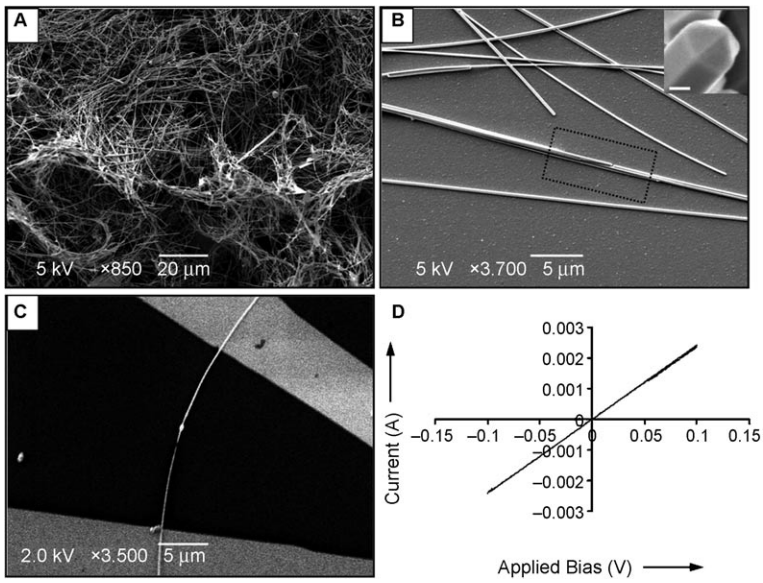

Figure 3. A) SEM image of as-synthesized gold nanowires. B) HREM)image of the gold nanowires. The marked area shows that the nanowires assemble into stacks (Inset: SEM image of a nanowire showing {111} end facets. Scale bar represents 50 nm). C) SEM image of a nanowire device. D) A typical current–voltage curve for the device shown in (C).

lective interactions between the two different amine molecules and growth sites on the side edges and faces).[33] We also measured the electrical properties of the Au nanowires. Figure 3C shows a SEM image of a single-nanowire device. Room-temperature two-point electrical measurements were made on six different Au nanowires. Figure 3D shows a typical current–voltage (I–V) curve obtained for the device at room temperature shown in Figure 3C with a 150-nm-diameter nanowire bridging the electrode junctions. Analysis of the I–V curve indicates a resistivity ($1.4\times10^{-5}\,\Omega\,cm$) similar to the intrinsic value of bulk gold ($2.2\times10^{-6}\,\Omega\,cm$).

XRD analysis further provides the structural information and evidence of the crystallinity of the as-synthesized Au particles, plates, and nanowires. Typical XRD patterns are compiled in Figure 4. All peaks can be assigned to diffraction from the (111), (200), (220), (311), and (222) planes of fcc gold, respectively. It is noted that the intensity ratio between the (200) and (111) peaks decreases upon increasing concentration of the quaternary amine, as shown in Figure 4A–C. The intensity ratio between the (220) and (111) peaks also exhibits a similar trend. In contrast, XRD of the thin Au plates shows predominant (111) and (222) peaks, which are expected for crystals with {111}-dominant facets oriented parallel to the surface of the supporting substrate (Figure 4D). The XRD pattern of the nanowires shows a pattern similar to that reported for single-crystal gold nanowires (Figure 4E).[15]

To verify the presence of capping molecules bound to the crystal surface, the crystals synthesized with varied molar ratios of DDAB and DA were examined by XPS. Figure 5 shows the XPS spectra of the N 1s core levels obtained from crystals synthesized with $\gamma=0$, 1.25, and 3, respectively. The N 1s XPS spectrum of the DA-capped ($\gamma=0$) Au crystals shows a characteristic peak at 401.1 eV, which is in agreement with the value reported in previous studies (Figure 5A).[34] It should be noted that the N 1s peak for the noncoordinated $-NH_2$-terminated alkyl amine is located at 399.3 eV.[34] Obviously, the calculated chemical shift occurs after the DA molecules are adsorbed on the Au crystals, indicating a strong interaction between the molecules and the Au surface. As γ increases to 1.25, the N 1s XPS spectrum shows two characteristic components with a signal intensity ratio of 1:1 (Figure 5B). The peak at 401.0 eV corresponds to primary amines capped on the Au substrate, while the other peak at 402.4 eV is

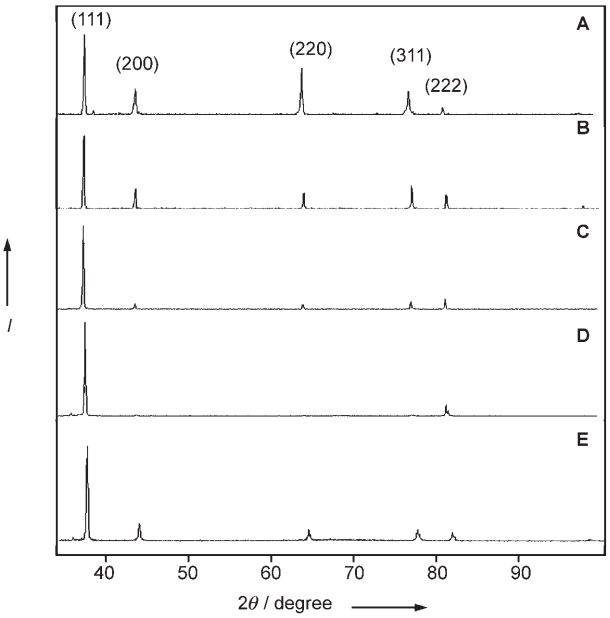

Figure 4. X-ray diffraction patterns of gold crystals: A) DA-coated particles. B) DDAB/DA-coated particles ($\gamma=1.25$). C) DDAB/DA-coated platelets ($\gamma=3$). D) DDAB/dibutylamine-coated thin plates. E) DDAB/trioctylamine-coated nanowires.

characteristic of quaternary amines adsorbed on the Au substrate.[35] In contrast, the N 1s XPS spectrum of the gold platelets ($\gamma=3$) shows two similar resonances to those shown in Figure 5B, but with an intensity ratio of 3.25:1 (quaternary amine/primary amine), comparable to the amine ratio used in the synthetic process (Figure 5C).

The distribution of particle morphologies observed in these experiments is determined not simply by the relative

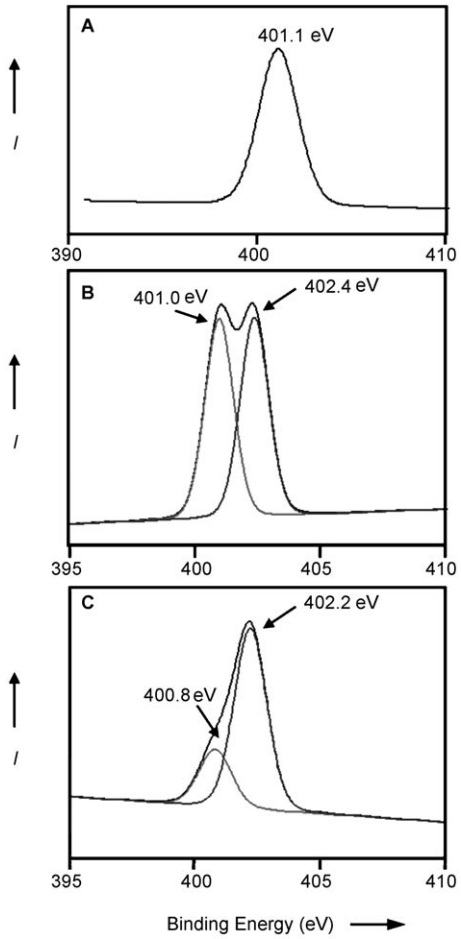

Figure 5. XPS N 1s spectra of gold crystals: A) DA-coated particles. B) DDAB/DA-coated particles ($\gamma = 1.25$). C) DDAB/DA-coated platelets ($\gamma = 3$).

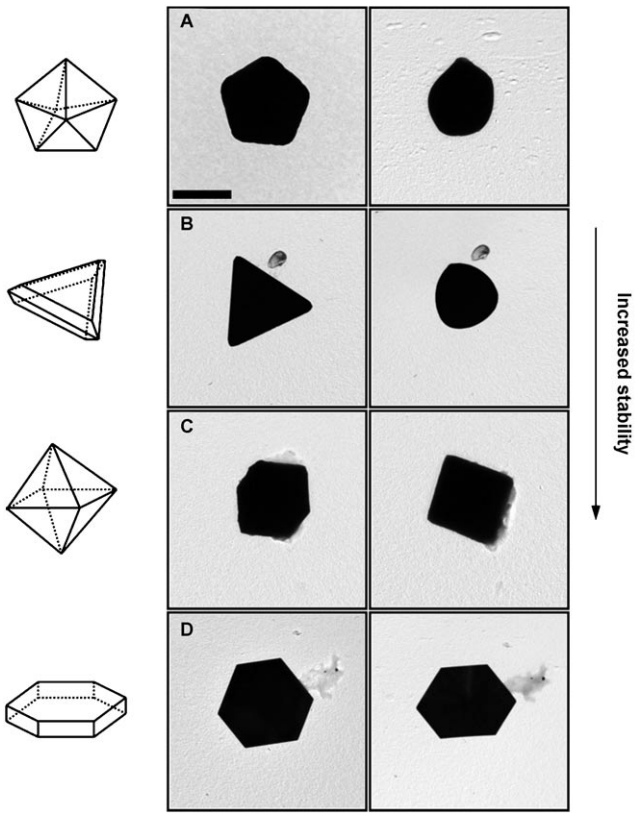

Figure 6. A series of TEM images of as-prepared microscale crystals (first column) and images taken after electron-beam irradiation for 20 s (second column). Note that images C and D (second column) were taken from -45° and 29° tilting angles, respectively. The scale bar represents 1 μm and applies to all images.

energies (thermodynamics) of the different structures, but also by the magnitudes of the energy barriers between different structures and the kinetics of structural changes. The isolation of particles in the form of a pentagonal decahedron up to a few micrometers in dimensions is surprising because these multiply twinned particles (MTPs),[30] which suffer from internal stress, may be stable only at very small sizes (typically under a few-hundred angstroms in diameter) according to detailed theoretical studies.[28] Beyond this critical size range, the particles contain a low angle boundary and are almost certainly metastable.[28] Indeed, it was observed that the as-prepared MTPs (truncated triangles and octahedra) readily melted and recrystallized in different structures upon electron-beam irradiation when the particles were supported on an insulating carbon layer (Figure 6A–C). The hexagonal plates did not melt under the same observation conditions (Figure 6D). On the basis of the melting analysis of large quantities of particles of similar size, the relative stability of the structures was established in decreasing order: hexagonal plate, octahedron, triangle, and pentagonal decahedron.

In conclusion, we report here an example of the direct, bottom-up synthesis of micrometer-sized gold crystals with well-defined morphologies. Our results suggest a general strategy for the scalable synthesis of large-sized metallic crystals: utilization of molecular recognition at the crystallographic planes under slow-growth conditions. The reaction and product are important not only because they provide a route to large crystals for a wide variety of applications, but also because they shed light on fundamental mechanisms that govern nanometer- and micrometer-scale phenomena in crystallization.

Experimental Section

In a typical synthesis of microscale particles, didodecyldimethylammonium bromide (DDAB: 65.2 mg; 0.141 mmol) and $H[AuCl_4]$ (18 mg; 0.045 mmol) were dissolved in toluene (10 mL), followed by addition of dodecylamine (DA: 21 mg; 0.113 mmol). The resulting mixture was heated at 81 °C for 34 h to give a golden precipitate, which was collected, washed with ethanol, and dried in air. A similar process was employed for the synthesis of Au plates, except that an excess of quaternary amine (DDAB: 145 mg; 0.339 mmol) was used. Gold octahedra, thin plates, and nanowires were synthesized according to the above-mentioned procedure except for the use of TDAC/DA (78 mg/42 mg), DDAB/dibutylamine (95 mg/38 μL) and DDAB/trioctylamine (95 mg/98 μL), respectively. The crystallographic

phase of the products was determined by powder XRD (Rigaku RU300, CuKα radiation). The sample microstructures and phases were further investigated by scanning electron microscopy and energy-dispersive X-ray spectroscopy (SEM/EDX, JEOL 5910), field-emission SEM (JEOL 6320FV), and transmission electron microscopy (Philips EM-420T). XPS spectra were recorded using an Omicron ESCA probe operated under vacuum at around 4.8×10^{-10} Torr with a monochromated AlKα radiation source (1486.6 eV, 300 W). Binding energies of the XPS spectra were corrected by referencing the C 1s peak of adventitious hydrocarbon to 284.8 eV. The pass energy of the analyzer was set at 25 eV. The particle-melting experiments were performed on a Philips EM-420T microscope operating at 200 kV. TEM samples of individual crystals were prepared by dropping dilute solutions of gold crystals in toluene onto 400-mesh carbon-coated copper grids and evaporating the solvent. Electrical characterization of the gold nanowires was performed using a Cascade Microtech microprobe station and an Agilent 4155C Semiconductor Parameter Analyzer.

Keywords:
amines · electron microscopy · gold · microcrystals · molecular recognition

[1] S. Mann, G. A. Ozin, *Nature* **1996**, *382*, 313.
[2] M. A. El-Sayed, *Acc. Chem. Res.* **2001**, *34*, 257.
[3] R. Shenhar, V. M. Rotello, *Acc. Chem. Res.* **2003**, *36*, 549.
[4] E. E. Oren, C. Tamerler, M. Sarikaya, *Nano Lett.* **2005**, *5*, 415.
[5] S. R. Whaley, D. S. English, E. L. Hu, P. F. Barbara, A. M. Belcher, *Nature* **2000**, *405*, 665.
[6] N. R. Jana, L. Gearheart, C. J. Murphy, *Adv. Mater.* **2001**, *13*, 1389.
[7] F. Kim, S. Kwan, J. Akana, P. D. Yang, *J. Am. Chem. Soc.* **2001**, *123*, 4360.
[8] B. R. Martin, D. J. Dermody, B. D. Reiss, M. M. Fang, L. A. Lyon, M. J. Natan, T. E. Mallouk, *Adv. Mater.* **1999**, *11*, 1021.
[9] Y. G. Sun, B. Mayers, Y. N. Xia, *Adv. Mater.* **2003**, *15*, 641.
[10] J. Tanori, M. P. Pileni, *Langmuir* **1997**, *13*, 639.
[11] Y. G. Sun, Y. N. Xia, *Science* **2002**, *298*, 2176.
[12] F. Kim, S. Connor, H. Song, T. Kuykendall, P. D. Yang, *Angew. Chem.* **2004**, *116*, 3759; *Angew. Chem. Int. Ed.* **2004**, *43*, 3673.
[13] W. P. Lim, Z. Zhang, H. Y. Low, W. S. Chin, *Angew. Chem.* **2004**, *116*, 5803; *Angew. Chem. Int. Ed.* **2004**, *43*, 5685.
[14] Y. N. Xia, P. D. Yang, Y. G. Sun, Y. Y. Wu, B. Mayers, B. Gates, Y. D. Yin, F. Kim, H. Q. Yan, *Adv. Mater.* **2003**, *15*, 353.
[15] J. G. Wang, M. L. Tian, T. E. Mallouk, M. H. W. Chan, *J. Phys. Chem. B* **2004**, *108*, 841.
[16] R. C. Jin, Y. W. Cao, C. A. Mirkin, K. L. Kelly, G. C. Schatz, J. G. Zheng, *Science* **2001**, *294*, 1901.
[17] G. S. Metraux, Y. C. Cao, R. C. Jin, C. A. Mirkin, *Nano Lett.* **2003**, *3*, 519.
[18] S. H. Chen, D. L. Carroll, *Nano Lett.* **2002**, *2*, 1003.
[19] S. S. Shankar, A. Rai, B. Ankamwar, A. Singh, A. Ahmad, M. Sastry, *Nat. Mater.* **2004**, *3*, 482.
[20] E. Hao, R. C. Bailey, G. C. Schatz, J. T. Hupp, S. Y. Li, *Nano Lett.* **2004**, *4*, 327.
[21] S. H. Chen, Z. L. Wang, J. Ballato, S. H. Foulger, D. L. Carroll, *J. Am. Chem. Soc.* **2003**, *125*, 16186.
[22] D. J. Milliron, S. M. Hughes, Y. Cui, L. Manna, J. B. Li, L. W. Wang, A. P. Alivisatos, *Nature* **2004**, *430*, 190.
[23] T. Mokari, E. Rothenberg, I. Popov, R. Costi, U. Banin, *Science* **2004**, *304*, 1787.
[24] Y. W. Jun, Y. Y. Jung, J. Cheon, *J. Am. Chem. Soc.* **2002**, *124*, 615.
[25] B. Nikoobakht, M. A. El-Sayed, *Langmuir* **2001**, *17*, 6368.
[26] Z. L. Wang, R. P. Gao, B. Nikoobakht, M. A. El-Sayed, *J. Phys. Chem. B* **2000**, *104*, 5417.
[27] S. Kumar, T. Nann, *Small* **2006**, *2*, 316.
[28] M. Gillet, *Surf. Sci.* **1977**, *67*, 139.
[29] R. L. Whetten, J. T. Khoury, M. M. Alvarez, S. Murthy, I. Vezmar, Z. L. Wang, P. W. Stephens, C. L. Cleveland, W. D. Luedtke, U. Landman, *Adv. Mater.* **1996**, *8*, 428.
[30] L. D. Marks, *Rep. Prog. Phys.* **1994**, *57*, 603.
[31] J. Aizenberg, J. C. Weaver, M. S. Thanawala, V. C. Sundar, D. E. Morse, P. Fratzl, *Science* **2005**, *309*, 275.
[32] H. Hiramatsu, F. E. Osterloh, *Chem. Mater.* **2004**, *16*, 2509.
[33] C. J. Johnson, E. Dujardin, S. A. Davis, C. J. Murphy, S. Mann, *J. Mater. Chem.* **2002**, *12*, 1765.
[34] J. Sharma, S. Mahima, B. A. Kakade, R. Pasricha, A. B. Mandale, K. Vijayamohanan, *J. Phys. Chem. B* **2004**, *108*, 13280.
[35] M. Li, M. Xu, N. Li, Z. Gu, X. Zhou, *J. Phys. Chem. B* **2002**, *106*, 4197.

Received: May 4, 2006

